Dalton Transactions

Accepted Manuscript

ROYAL SOCIETY OF CHEMISTRY

www.rsc.org/dalton

Cite this: DOI: 10.1039/c0xx00000x

www.rsc.org/xxxxxx ARTICLE TYPE

p-type Mesoscopic NiO as an Active Interfacial Layer for Carbon Counter Electrodes Based Perovskite Solar Cells

Zonghao Liu,[a] Meng Zhang,[a] Xiaobao Xu,[a] Lingling Bu,[a] Wenjun Zhang,[a] Wenhui Li,[a] Zhixin Zhao,*[a] Mingkui Wang,*[a] Yi-Bing Cheng,[a,c] Hongshan He*[b]

Received (in XXX, XXX) Xth XXXXXXXXX 20XX, Accepted Xth XXXXXXXXX 20XX
DOI: 10.1039/b000000x

Replacement of ZrO_2 insulator layer in state-of-the-art TiO_2/ZrO_2/carbon structure by mesoscopic *p*-type NiO particles led to 39% increase of energy conversion efficiency of hole-conductor-free organometallic perovskite heterojunction solar cells with carbon counter electrodes. In these cells, the light absorber, $CH_3NH_3PbI_3$, formed instantly inside the pores of the entire TiO_2/NiO/carbon layer upon sequential deposition of PbI_2 and CH_3NH_3I. Photoluminescence, impedance spectroscopy and transient photovoltage decay measurements have revealed that introduction of NiO extended the electron lifetime and augmented the hole extraction to the counter electrode. As a result, the photocurrent and open-circuit voltage both increased, resulting in a cell with impressive energy conversion efficiency of 11.4% under AM1.5G condition.

Introduction

Organometal trihalide perovskite solar cells have shown promise as an efficient technology in utilization of solar energy.[1] In the past three years, perovskite-based mesoscopic or thin-film heterojunction solar cells have achieved power conversion efficiencies (PCE) as high as 17.9%.[2-4] However, stability, environmental friendliness as well fabrication cost, must be taken into account in order to make this type of device a viable solution for the conversion of solar energy to electricity. Theoretical studies show that the unique electronic structure and optical properties of perovskite materials contribute largely to their remarkable photovoltaic performance.[5-7, 8-13] Several exploratory investigation also indicates Sn may be an alternative to Pb, which is toxic and is the dominate source of peroviskite salt..[14-16] Recent studies further reveals the potential of mixed halogen perovskite,[17] modified TiO_2 with Sb_2S_3,[18] TiO_2-free oxide nanostructure,[19] carbon nanotube/polymer composites,[20] and layered hybrid perovskite[21] for improving the stability of Perovskite solar cells. The use of expensive organic hole-conductor materials as charge selective layers and a metal film (Au or Ag et al) as a counter electrode processed with vacuum evaporation techniques are also a potential hurdle for large-scale production and practical applications because of the high cost and complicated manufacturing process.[22-27] It is therefore desirable to develop perovskite solar cells using low-cost materials with simple manufacturing process.

p-Type inorganic materials such as CuI[28], CuSCN[29-31] and NiO[31-38] have been employed in perovskite solar cells. The simple synthetic methods, low-cost, and suitable energy levels make these materials appealing in cost-effective perovskite solar cells. However, the poor stability of CuI and CuSCN has been a concern due to their easy degradation.[39] NiO is an intrinsic nonstoichiometric p-type semiconductor with wide bandgap, good thermal and chemical stability.[40] NiO has been employed as photocathode materials in p-type dye-sensitized solar cells, p-n tandem dye sensitized solar cells, and a hole collector in organic bulk heterojunction solar cells.[39, 41-45] Recently, NiO has been used in perovskite heterojunction solar cells with efficiency,[31-37] in which, NiO acts as an electron blocking material because of its higher conduction band compared to $CH_3NH_3PbI_3$ (-1.8 eV vs. -3.93 eV).[31-36] Photo-induced absorption spectra and photoluminescence measurements also show that NiO can act as a hole conductor.[32, 46] Nevertheless, these devices employ expensive PCBM as electron selective electrode, which could be problematic for practical application and need to be addressed.

Low-cost carbon black/graphite materials have been used as counter electrode in dye-sensitized solar cells and showed good performance.[47-49] Ku *et al* reported HTMs-free perovskite solar cells with a carbon black/graphite counter electrode, and PCE of 6.64% is achived.[50] The performance of HTMs-free solar cells is further improved when highly ordered mesoporous carbon or TiO_2 nanosheets are employed.[51, 52] Recently, Han *et al* use 5-ammoniumvaleric acid iodide modified $CH_3NH_3PbI_3$ perovskite as an absorber in HTMs-free solar cell. The resulting device shows PCE of 12.8% with promising stability.[53] These results demonstrate that the potential of carbon materials as Earth-abundant materials for cost-effective perovskite heterojunction solar cells. In this HTM-free solar cell, the ZrO_2 was used as a insulator to separate TiO_2 layer and carbon layer. The perovskite $CH_3NH_3PbI_3$ transports holes to the counter electrode. Since the diffusion length of $CH_3NH_3PbI_3$ is ~100 nm, it is much smaller than the thickness of ZrO_2 layer (1-2 μm). This will restrain the further improvement of devices performance of HTM-free

perovskite solar cells.[54, 55]

This study communicates a strategy to address aforementioned issues. We fabricated perovskite heterojunction solar cell using p-type mesoscopic NiO as an interfacial layer and carbon black/graphite as counter electrode. In these cells, the mesoscopic pores are filled with $CH_3NH_3PbI_3$ by sequential deposition process.[2] The mesoscopic NiO layer acted as a hole conductor or electron blocking layer to suppress charge recombination and facilitate the hole extraction.[32, 46] This type solar cell using inorganic materials (coded as TiO_2/NiO($CH_3NH_3PbI_3$)/carbon) can be fabricated in atmospheric environment, showing a promising PCE of 11.4% under standard test conditions. To our best knowledge, this is the first report on efficient perovskite heterojunction solar cells using all inorganic p-type and n-type mesoscopic materials fabricated with screen printing technology.

Results and Discussion

The devices were fabricated by screen-printing mesoscopic TiO_2 layer, NiO interfacial layer, carbon/graphite materials layer-by-layer on compact TiO_2 coated FTO glass, followed by sequential deposition of PbI_2 and CH_3NH_3I. A schematic representation of the cell structure is shown in Fig. 1. In this configuration, the cell has a compact TiO_2 layer as a hole blocking layer between the FTO and the mesoscopic TiO_2 layer, a carbon layer as the counter electrode on the top of NiO layer. Upon absorbing light, $CH_3NH_3PbI_3$ perovskite generates exciton, which efficiently separates into electrons and holes because of a low exciton binging energy (being ~0.5 eV).[23, 56] The photo-generated electron injects into the conduction band (CB, -4.0 eV) of the TiO_2 and hole injects into the valence band (VB, -5.2 eV) of the mesoscopic NiO layer.[23, 32] This will be different from reported TiO_2/ZrO_2/($CH_3NH_3PbI_3$)/carbon device structure, in which ZrO_2 layer acted as an insulating separator between TiO_2 and carbon layer with no charge injection due to the mismatch of energy levels between $CH_3NH_3PbI_3$ and the ZrO_2.

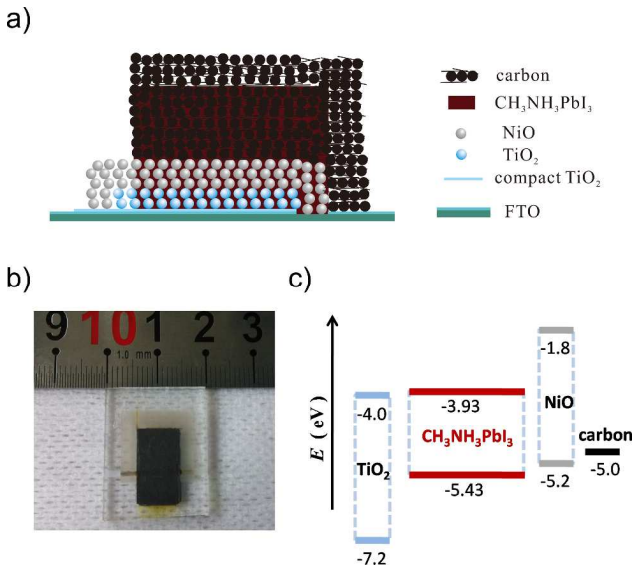

Fig. 1 a) Schematic representation of TiO_2/NiO($CH_3NH_3PbI_3$)/carbon device structure. b) Optical image of device. c) Schematic of the relative energy levels of each layer.

Fig. 2 shows a cross-sectional scanning electron microscopy (SEM) image of the fabricated device. Three active layers were observed. On the top of the FTO is a TiO_2 layer with thickness ~ 450 nm. On its top is a NiO layer with nice contact with TiO_2 layer. The NiO layer exhibits a mesoscopic structure with total thickness ~ 1 μm. The carbon/graphite covers the NiO layer with quite large pores. The large flakes of graphite are embedded inside carbon materials. The perovskite $CH_3NH_3PbI_3$ formed inside of the entire triple layers with uniform distribution as confirmed by the energy dispersive X-ray (EDAX) spectra as shown in Fig. S1.

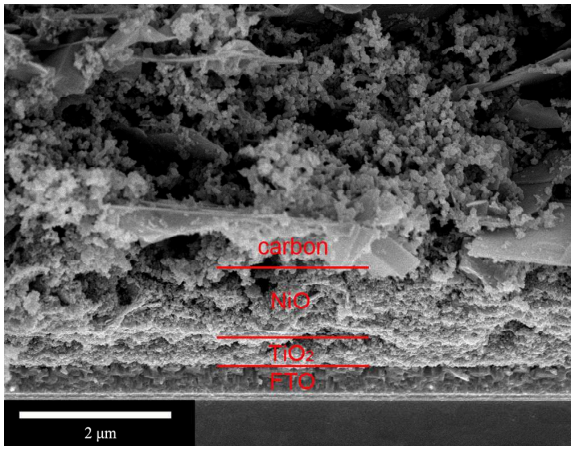

Fig. 2 Cross-sectional SEM image of the TiO_2/NiO($CH_3NH_3PbI_3$)/carbon device. The labels are used to indicate the layer structure, in which the $CH_3NH_3PbI_3$ is penetrated.

The photocurrent-voltage curve of the champion cell with a TiO_2/NiO($CH_3NH_3PbI_3$)/carbon structure is shown in Fig. 3a. The device exhibited PCE of 11.4% with a J_{SC} of 18.2 mA cm^{-2}, a V_{OC} of 890 mV, and a FF of 0.71. As a comparison, a cell with TiO_2/ZrO_2($CH_3NH_3PbI_3$)/carbon device was also fabricated and tested under same condition. Its photocurrent-voltage curve was also shown in Fig. 3a. The results showed a significant increase in V_{OC}, J_{SC} and FF when ZrO_2 was replaced by NiO. Fig. 3b shows the incident photon to electron conversion efficiency (IPCE) of the two devices. Compared to TiO_2/ZrO_2 ($CH_3NH_3PbI_3$)/carbon device, replacement of ZrO_2 by NiO resulted in a cell with higher IPCE values in the range from 400 to 800 nm. The calculated photocurrent from the IPCE spectrum gives a current density of 17.7 mA/cm^2 for a NiO device and 15.9 mA/cm^2 for a ZrO_2 device, respectively. These data are in agreement with the measured photocurrent densities. Since TiO_2/ZrO_2($CH_3NH_3PbI_3$) and TiO_2/NiO($CH_3NH_3PbI_3$) films exhibited almost identical absorption spectra in the range of 400-800 nm as shown in Fig. S2, the TiO_2/NiO($CH_3NH_3PbI_3$)/carbon device clearly posses higher charge seperation or charge collection efficiency than the devcie with ZrO_2. The complete devices performance distribution of all devices is described in Fig. S3 and Fig. S4. The stability of TiO_2/NiO ($CH_3NH_3PbI_3$)/carbon devices was investigated in dark. Fig. S5 shows the evolution of device photovoltaic parameters, which were prolonged in dark at ambient temperature.

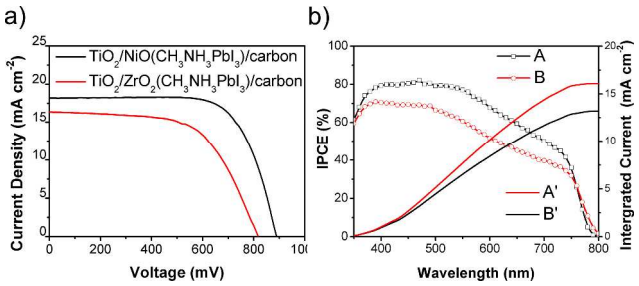

Fig. 3 a) Current-Voltage characteristics of $TiO_2/NiO(CH_3NH_3PbI_3)$ /carbon device (black line) and $TiO_2/ZrO_2(CH_3NH_3PbI_3)$/carbon device (red line). b) IPCE spectra of $TiO_2/NiO(CH_3NH_3PbI_3)$/carbon device (line A) and $TiO_2/ZrO_2(CH_3NH_3PbI_3)$/carbon device (line B). Integrated current of $TiO_2/NiO(CH_3NH_3PbI_3)$/carbon device (line A′) and $TiO_2/ZrO_2(CH_3NH_3PbI_3)$/carbon device (line B′).

Table 1 Device performance of $TiO_2/NiO(CH_3NH_3PbI_3)$/carbon device and $TiO_2/ZrO_2(CH_3NH_3PbI_3)$/carbon device measured under simulated AM 1.5 (100 mW cm^{-2}) condition.

Device		J_{SC}(mA cm^{-2})	V_{OC}(mV)	ff	η (%)
TiO_2/NiO/C	champion	18.2	890	0.71	11.4
	average [a]	15.4	871	0.70	9.4
TiO/ZrO_2/C	champion	16.4	818	0.60	8.2
	average [b]	13.3	824	0.60	6.6

[a] Average device performance parameter were calculated with a standard deviation from 24 $TiO_2/NiO(CH_3NH_3PbI_3)$/carbon devices; [b] Average device performance parameter were calculated with a standard deviation from 24 $TiO_2/ZrO_2(CH_3NH_3PbI_3)$/carbon devices. The complete devices performance distribution of all devices is described in Fig. S3 and Fig. S4.

As shown in Fig. 4, a fast photoluminescence (PL) quenching process was observed for the $TiO_2(CH_3NH_3PbI_3)$ and $NiO(CH_3NH_3PbI_3)$ films. The obtained lifetimes (τ_e) of the photo-generated carriers (quoted as the time taken to reach 1/e of the initial intensity) were 5.3, and 2.3 ns for $NiO(CH_3NH_3PbI_3)$, and $TiO_2(CH_3NH_3PbI_3)$ films, respectively. Both were significantly lower than that of $ZrO_2(CH_3NH_3PbI_3)$ film (24 ns). This result confirmed fast interfacial charge transfer processes occurred after the films were excited. [46, 54, 55] For $TiO_2(CH_3NH_3PbI_3)$ film, this process involved the electron injection from the CB of $CH_3NH_3PbI_3$ to the CB of TiO_2[26, 54, 55] because of its lower energy level. For $NiO(CH_3NH_3PbI_3)$ film, situation may become complicated. This is because the CB of NiO is significant higher (-1.8 eV vs. -3.93 eV), but its VB energy level is quite close to that of $CH_3NH_3PbI_3$. Therefore NiO might mainly behave as a hole conductor. Therefore, the PL quenching may come from the hole injection from VB of $CH_3NH_3PbI_3$ to the VB of NiO.[26, 54, 55] Concurrently, the TiO_2 underneath the NiO blocks the flow of holes at the $TiO_2/CH_3NH_3PbI_3$ interface between two materials due to the large VB energy levels difference (-3.93 eV vs. -7.2 eV). This is consistent with Malinkiewicz's report on organic charge-transport layer-based perovskite solar cells using polyTPD and PCBM as an electron and a hole blocking layer, respectively.[27]

Measurements of photovoltage and short circuit current of devices under different light intensities indicated different interfacial charge recombination process. It was found the J_{SC} exhibited a linear response to light intensities; whereas V_{OC} displayed a linear response to the logarithm of incident photo flux as shown in Fig. S6. The slope of the photovoltage versus the logarithm of incident photo flux for a solar cell with an ideal photodiode behaviour is expected to be 59 mV/decade at 300K. [57] However, the slopes for $TiO_2/NiO(CH_3NH_3PbI_3)$/carbon device and $TiO_2/ZrO_2(CH_3NH_3PbI_3)$/carbon device were found to be -173 mV/decay and -240 mV/decay, respectively. This result indicates that the loss of photogenerated electron in $TiO_2/ZrO_2(CH_3NH_3PbI_3)$/carbon device is faster than that of $TiO_2/NiO(CH_3NH_3PbI_3)$/carbon device. This further indicates different interfacial charge recombination processes between these two devices, which are responsible for their photovoltage.[57]

Electronic impedance measurement (IS) showed a large charge recombination resistance at photoactive layer interfaces in $TiO_2/NiO(CH_3NH_3PbI_3)$/carbon device. In dark IS measurement, with the applied bias from the working electrode of the IS system, the injected electrons from the FTO contact transport through mesoporousTiO_2, diffuse within the $CH_3NH_3PbI_3$, and eventually reach the carbon counter electrode. The Nyquist plots of $TiO_2/NiO(CH_3NH_3PbI_3)$/carbon device and $TiO_2/ZrO_2(CH_3NH_3PbI_3)$/carbon device showed two main features: (i) the arc at high frequency region assigned to charge transfer process at carbon counter electrode interface as this process is very fast; and (ii) the arc at low frequency region assigned to the charge recombination process at the photoactive interface as this process is slow.[58-60] Fig. 5a presents the recombination resistance (R_{rec}) from impedance measurements in devices as a function of the bias. The Nyquist plots were shown in Fig. S7. The $TiO_2/NiO(CH_3NH_3PbI_3)$/carbon device displayed larger R_{rec} than that of TiO_2/ZrO_2 ($CH_3NH_3PbI_3$)/carbon device, indicating that charge recombination is slower in the former. Fig. 5b presents the resistance (R_{CE}) for the charge transfer process related to the counter electrode as a function of dark current. It was found that the $TiO_2/NiO(CH_3NH_3PbI_3)$/carbon device exhibited lower R_{CE} than that of TiO_2/ZrO_2 ($CH_3NH_3PbI_3$)/carbon device at a given current. This result indicates that charge transfer process at the counter electrode is much efficient when NiO was used. In the case of device with ZrO_2, $CH_3NH_3PbI_3$ acts as hole transporting material and participates in the hole extraction to the counter electrode.[50, 61, 62] However, in the case of device with NiO, the hole transporting property of NiO layer could benefit the hole extraction and collection efficiency.[46] Therefore, the $TiO_2/NiO(CH_3NH_3PbI_3)$/carbon device presented a higher fill factor.

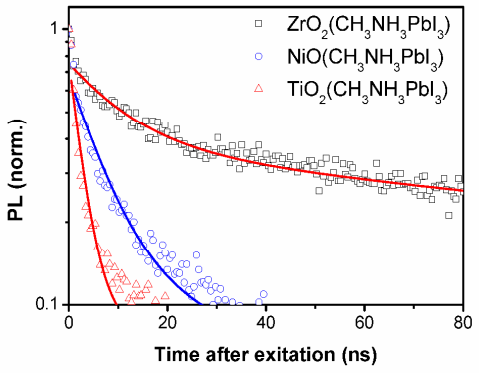

Fig. 4 Time-resolved PL decays of $ZrO_2/CH_3NH_3PbI_3$ film (black square), $NiO/CH_3NH_3PbI_3$ film (blue circle), $TiO_2/CH_3NH_3PbI_3$ film (red triangle). Excitation wavelength: 443 nm.

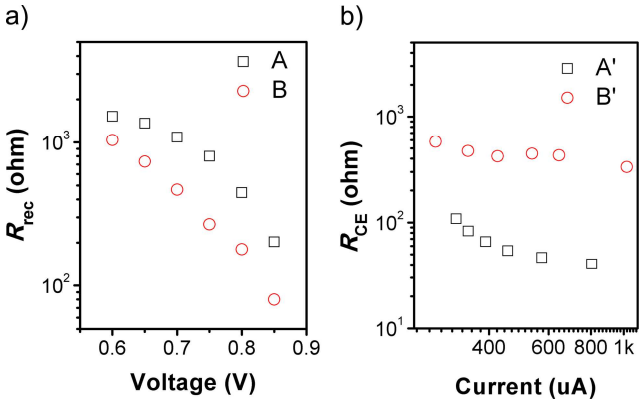

Fig. 5 a) Charge recombination resistance (R_{rec}) of $TiO_2/NiO(CH_3NH_3PbI_3)$/carbon (dots A) and $TiO_2/ZrO_2(CH_3NH_3PbI_3)$/carbon device (dots B) versus applied potential from impedance measurement in the dark. b) Charge transfer resistance (R_{rec}) at the counter electrode interface of $TiO_2/NiO(CH_3NH_3PbI_3)$/carbon device (dots A') and TiO_2/ZrO_2 ($CH_3NH_3PbI_3$)/carbon device (dots B') from impedance measurements in the dark.

The use of NiO increased the electron lifetime of the resulting devices. Fig. 6 presents the electron lifetime as a function of the incident light intensity from transient photovoltage decay measurements.[63, 64] It was observed that electron lifetime of $TiO_2/NiO(CH_3NH_3PbI_3)$/carbon device was longer than that of $TiO_2/ZrO_2(CH_3NH_3PbI_3)$/carbon device. This may be attributed to the dual function of NiO as a hole conductor and its electron blocking property.[32, 46] Therefore, the remarkable improvement of device performance for $TiO_2/NiO(CH_3NH_3PbI_3)$/carbon device can be attributed to the NiO layer. In TiO_2/ZrO_2 ($CH_3NH_3PbI_3$)/carbon device, the photo-generated electron can be fast injected to the CB of TiO_2, as evidenced by a quick quenching of the photoluminescence emission for perovskite/TiO_2 in Fig. 4. The injected electron transports through the TiO_2 mesoporous network to the external circuit. Meanwhile, the photo-generated hole transports through the perovskite to the counter electrode due to the ambipolar charge transport properties of perovskite.[50, 54, 55, 61] However, in $TiO_2/NiO(CH_3NH_3PbI_3)$/carbon device the situation could be different. In accompany with electron injection and transporting in TiO_2, the photo-generated hole can be fast injected to the VB of NiO and diffuse in this layer (see Fig. 2), which directly connects to the counter electrode.[32, 46] Nevertheless, the $CH_3NH_3PbI_3$ heterojunction using mesoporous NiO interfacial layer was demonstrated to efficiently convert photon into electricity. More studies are necessary to carry out in the near future for a more precise knowledge about the specific device.

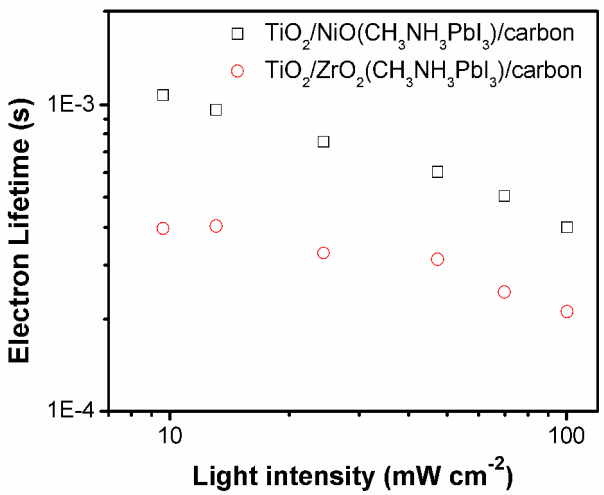

Fig. 6 Electron lifetime versus light intensity from transient photovoltage decay measurements.

Conclusions

In summary, we have demonstrated an efficient pervoskite heterojunction solar cell using p-type mesoscopic NiO as an interfacial layer. This type of solar cell using all inorganic p-type and n-type materials can be fabricated in atmospheric environment, presenting a promising power conversion efficiency of 11.4%. The open-circuit voltage, short-circuit current and fill factor of the $TiO_2/NiO(CH_3NH_3PbI_3)$/carbon device were significantly improved than the counterpart devices using mesoscopic ZrO_2 layer as separator, which was attributed to the enlarged electron lifetime and augmented interfacial charge transfer process on the carbon counter electrode because of the dual functions as an electron blocker and a hole conductor. This offers a viable pathway to develop efficient low-cost solar cells with attractive properties for scale up and practical applications.

Experimental Section

Device fabrication

Fabrication of $TiO_2/NiO(CH_3NH_3PbI_3)$/carbon device: FTO conducting glass were etched with sander to form two detached electrode patterns before being ultrasonically cleaned with detergent solution, deionized water and ethanol successively. A compact TiO_2 layer was deposited on the cleaned FTO glass by spray pyrolysis deposition with di-isopropoxytitanium bis(acetyl acetonate) solution at 450°C. The films were sintered at 500°C for 30 min and then cooled to room temperature. A 450 nm mesoporous TiO_2 (DSL. 18NR-T, 20 nm, Dyesol, Australia, diluted at 1/3.5 mass ratio of paste/terpineol) layer, a 1 µm NiO hole-conductor layer (NiO paste was used according to our previous report about p-type dye-sensitized solar cells)[44] and a 8 µm carbon black/graphite layer (black/graphite mass ratio 1/4, prepared according literature)[52] were subsequently prepared by screen printing onto FTO conducting glass layer by layer, which were sintered at 500°C, 500°C and 400°C for 30 min respectively. After that, the resulted films were infiltrated with PbI_2 by dropping a PbI_2 solution in DMF (462 mg ml^{-1}) that was kept at 70°C. After drying, the films were dipped into 2-propanol for 1-2

s before being dipped in a solution of CH_3NH_3I in 2-propanol (10 mg ml^{-1}) for 10 min and then rinsed with 2-propanol and the films changed colour from light yellow to black during the dipping process, indicating the formation of the perovskite $CH_3NH_3PbI_3$. After drying, the fabrication of the device was finished.

Fabrication of TiO_2/ZrO_2($CH_3NH_3PbI_3$)/carbon device: The device structure was prepared through substituting NiO hole-conductor layer with a 1 μm ZrO_2 spacer layer according to the procedure described above for the fabrication of TiO_2/NiO($CH_3NH_3PbI_3$)/carbon device.

Devices Characterization

A xenon light source solar simulator (450W, Oriel, model 9119) with AM 1.5G filter (Oriel, model 91192) was used to give an irradiance of 100 mW cm^{-2} at the surface of the solar cells. The current-voltage characteristics of the devices under these conditions were obtained by applying external potential bias to the devices and measuring the generated photocurrent with a Keithley model 2400 digital source meter (Keithley, USA). A similar data acquisition system was used to control the incident photon-to-current conversion efficiency (IPCE) measurement. A white light bias (1% sunlight intensity) was applied onto the devices during the IPCE measurements with AC model (10 Hz). The devices (~0.6 cm^2) were tested using a metal mask to prevent the scattering light.

Time-Resolved Fluorescene Decay Measurements

Time-resolved fluorescence decays measurements were recorded on a FLSP920 spectrometer (Edinburgh instruments, Inc.). A picosecond pulsed light-emitting diode centered (443 nm) with a frequency of 10 MHz was used. The NiO, TiO_2 and ZrO_2 nanoparticles were screen-printed on quartz substrates to form 0.8 μm thick films. After sintered at 500 ^oC for 30 min, the resulted films were infiltrated with PbI_2 by spin coating (6500 rmp for 60s) a PbI_2 solution in DMF (462 mg ml^{-1}) that was kept at 70^oC. After drying, the films were dipped in 2-propanol for 1-2 s before being dipped in the solution of CH_3NH_3I in 2-propanol (10 mg ml^{-1}) for 60 s and then rinsed with 2-propanol. It is worth noting that the films changed colour from light yellow to black during the dipping process, indicating the formation of the perovskite $CH_3NH_3PbI_3$.

Electrochemical Impedance Measurements and Transient Decay Measurements

Electronic impedance spectroscopy (IS) was carried out on ZAHNER ENNIUM Electrochemical Workstations in the frequency range 100 mHz to 2 M Hz with 10 mV AC amplitude in dark. The electron lifetime was determined by transient photovoltage decay measurements. For the photovoltage transient decay measurement, an array of diodes was used to produce a white light bias and blue-light diodes controlled by a fast solid-state switch was used to generate a pulse (0.05 s square pulse-width, 100 ns rise and fall time). The voltage dynamics were recorded on a PC-interfaced Keithley 2602A source meter with a 100 μs response time. The perturbation light source was set to a suitably low level for the voltage-decay kinetics to be monoexponential. By varying the intensity of white-light bias, the recombination rate constant and the electron diffusion rate constant could be estimated over a range of applied biases, which were used to evaluate the electron lifetime of the devices.

Acknowledgment

This work was partially supported by the National Basic Research Program of China (973 program 2011CBA00703), the Fundamental Research Funds for the Central Universities (Grant No. HUST: 2014TS016), NSFC (21103057), the CME with the Program of New Century Excellent Talents in University (NCET-10-0416) (ZZ), and Council on Faculty Research, and the President's Fund for Research and Creative Activity, Eastern Illinois University (HH).

Notes and references

[a] *Michael Grätzel Center for Mesoscopic Solar Cells, Wuhan National Laboratory for Optoelectronics, School of Optical and Electronic Information, Huazhong University of Science and Technology, Wuhan, Hubei 430074, PR China;*
[b] *Department of Chemistry, Eastern Illinois University, Charleston, Illinois 61920, United States;*
[c] *Department of Materials Engineering, Monash University, Melbourne, Victoria 3800, Australia.*

† Electronic Supplementary Information (ESI) available: EDAX spectra of the TiO_2/NiO($CH_3NH_3PbI_3$)/carbon device, absorbance of the TiO_2/NiO($CH_3NH_3PbI_3$) films and TiO_2/ZrO_2($CH_3NH_3PbI_3$) films, the complete device performance distribution of all devices, photocurrent and photovoltage response of devices under different light intensity, Nyquist plots of devices obtained in dark. See DOI: 10.1039/b000000x/

1. A. Kojima, K. Teshima, Y. Shirai and T. Miyasaka, *J. Am. Chem. Soc.*, 2009, **131**, 6050-6051.
2. J. Burschka, N. Pellet, S. Moon, R. Humphry-Baker, P. Gao, M. K. Nazeeruddin and M. Grätzel, *Nature*, 2013, **499**, 316-319.
3. M. Liu, M. B. Johnston and H. J. Snaith, *Nature*, 2013, **501**, 395-398.
4. N. J. Jeon, H. G. Lee, Y. C. Kim, J. Seo, J. H. Noh, J. Lee and S. I. Seok, *J. Am. Chem. Soc.*, 2014, **136**, 7837-7840.
5. J. M. Frost, K. T. Butler, F. Brivio, C. H. Hendon, M. van Schilfgaarde and A. Walsh, *Nano Lett.*, 2014, **14**, 2584-2590.
6. A. Amat, E. Mosconi, E. Ronca, C. Quarti, P. Umari, M. K. Nazeeruddin, M. Grätzel and F. De Angelis, *Nano Lett.*, 2014, **14**, 3608-3616.
7. F. Brivio, K. T. Butler, A. Walsh and M. van Schilfgaarde, *Phys. Rev. B*, 2014, **89**, 155204.
8. A. Stroppa, P. Jain, P. Barone, M. Marsman, J. M. Perez-Mato, A. K. Cheetham, H. W. Kroto and S. Picozzi, *Angew.Chem.Int.Ed.*, 2011, **50**, 5847-5850.
9. J. M. Frost, K. T. Butler and A. Walsh, *APL Mat.*, 2014, **2**, 81506.
10. D. Di Sante, A. Stroppa, P. Jain and S. Picozzi, *J. Am. Chem. Soc.*, 2013, **135**, 18126-18130.
11. Y. Kutes, L. Ye, Y. Zhou, S. Pang, B. D. Huey and N. P. Padture, *J. Phys. Chem. Lett.*, 2014, **5**, 3335-3339.
12. M. A. Green, A. Ho-Baillie and H. J. Snaith, *Nat. Photonics.*, 2014, **8**, 506-514.
13. Y. Tian, A. Stroppa, Y. Chai, L. Yan, S. Wang, P. Barone, S. Picozzi and Y. Sun, *Sci. Rep.*, 2014, **4**, 6062.
14. F. Hao, C. C. Stoumpos, D. H. Cao, R. P. H. Chang and M. G. Kanatzidis, *Nat. Photonics.*, 2014, **8**, 489-494.
15. N. K. Noel, S. D. Stranks, A. Abate, C. Wehrenfennig, S. Guarnera, A. Haghighirad, A. Sadhanala, G. E. Eperon, S. K. Pathak, M. B. Johnston, A. Petrozza, L. M. Herz and H. J. Snaith, *Energy Environ. Sci.*, 2014, **7**, 3061-3068.
16. Y. Ogomi, A. Morita, S. Tsukamoto, T. Saitho, N. Fujikawa, Q. Shen, T. Toyoda, K. Yoshino, S. S. Pandey, T. Ma and S. Hayase, *J. Phys. Chem. Lett.*, 2014, **5**, 1004-1011.
17. J. H. Noh, S. H. Im, J. H. Heo, T. N. Mandal and S. I. Seok, *Nano Lett.*, 2013, **13**, 1764-1769.
18. S. Ito, S. Tanaka, K. Manabe and H. Nishino, *J. Phys. Chem.*

C, 2014, **118**, 16995-17000.
19. T. Leijtens, G. E. Eperon, S. Pathak, A. Abate, M. M. Lee and H. J. Snaith, *Nat. Commun.*, 2013, **4**, 2885.
20. S. N. Habisreutinger, T. Leijtens, G. E. Eperon, S. D. Stranks, R. J. Nicholas and H. J. Snaith, *Nano Lett.*, 2014, **14**, 5561-5568.
21. I. C. Smith, E. T. Hoke, D. Solis-Ibarra, M. D. McGehee and H. I. Karunadasa, *Angew. Chem. Int. Ed.*, 2014, **53**, 11232-11235.
22. M. M. Lee, J. Teuscher, T. Miyasaka, T. N. Murakami and H. J. Snaith, *Science*, 2012, **338**, 643-647.
23. H. Kim, C. Lee, J. Im, K. Lee, T. Moehl, A. Marchioro, S. Moon, R. Humphry-Baker, J. Yum, J. E. Moser, M. Grätzel and N. Park, *Sci. Rep.*, 2012, **2**, 259.
24. J. H. Heo, S. H. Im, J. H. Noh, T. N. Mandal, C. Lim, J. A. Chang, Y. H. Lee, H. Kim, A. Sarkar, M. K. Nazeeruddin, M. Grätzel and S. I. Seok, *Nat. Photonics.*, 2013, **7**, 486-491.
25. D. Bi, L. Yang, G. Boschloo, A. Hagfeldt and E. M. J. Johansson, *J. Phys. Chem. Lett.*, 2014, **4**, 1532-1536.
26. P. Docampo, J. M. Ball, M. Darwich, G. E. Eperon and H. J. Snaith, *Nat. Commun.*, 2013, **4**, 2761.
27. O. Malinkiewicz, A. Yella, Y. H. Lee, G. M. Espallargas, M. Gratzel, M. K. Nazeeruddin and H. J. Bolink, *Nat. Photonics.*, 2014, **8**, 128-132.
28. J. A. Christians, R. C. M. Fung and P. V. Kamat, *J. Am. Chem. Soc.*, 2014, **136**, 758-764.
29. S. Ito, S. Tanaka, H. Vahlman, H. Nishino, K. Manabe and P. Lund, *Chemphyschem*, 2014, **15**, 1194-1200.
30. P. Qin, S. Tanaka, S. Ito, N. Tetreault, K. Manabe, H. Nishino, M. K. Nazeeruddin and M. Grätzel, *Nat. Commun.*, 2014, **5**, 3834.
31. A. S. Subbiah, A. Halder, S. Ghosh, N. Mahuli, G. Hodes and S. K. Sarkar, *J. Phys. Chem. Lett.*, 2014, **5**, 1748-1753.
32. K. Wang, J. Jeng, P. Shen, Y. Chang, E. W. Diau, C. Tsai, T. Chao, H. Hsu, P. Lin, P. Chen, T. Guo and T. Wen, *Sci. Rep.*, 2014, **4**, 4756.
33. J. Jeng, K. Chen, T. Chiang, P. Lin, T. Tsai, Y. Chang, T. Guo, P. Chen, T. Wen and Y. Hsu, *Adv. Mater.*, 2014, **26**, 4107-4113.
34. Z. Zhu, Y. Bai, T. Zhang, Z. Liu, X. Long, Z. Wei, Z. Wang, L. Zhang, J. Wang, F. Yan and S. Yang, *Angew. Chem. Int. Ed.*, 2014, 10-1002.
35. K. Wang, P. Shen, M. Li, S. Chen, M. Lin, P. Chen and T. Guo, *ACS Appl. Mater. Interfaces*, 2014, 10-1021.
36. L. Hu, J. Peng, W. Wang, Z. Xia, J. Yuan, J. Lu, X. Huang, W. Ma, H. Song, W. Chen, Y. Cheng and J. Tang, *ACS Photonics*, 2014, **1**, 547-553.
37. H. Tian, B. Xu, H. Chen, E. M. J. Johansson and G. Boschloo, *ChemSusChem*, 2014, 10-1002.
38. H. Wang, X. Zeng, Z. Huang, W. Zhang, X. Qiao, B. Hu, X. Zou, M. Wang, Y. Cheng and W. Chen, *ACS Appl. Mater. Interfaces*, 2014, 10-1021.
39. J. Bandara and H. Weerasinghe, *Sol. Energy Mater. Sol. Cells*, 2005, **85**, 385-390.
40. F. Odobel, L. Le Pleux, Y. Pellegrin and E. Blart, *Acc. Chem. Res.*, 2010, **43**, 1063-1071.
41. M. D. Irwin, D. B. Buchholz, A. W. Hains, R. P. H. Chang and T. J. Marks, *PNAS*, 2008, **105**, 2783-2787.
42. J. He, H. Lindström, A. Hagfeldt and S. Lindquist, *J. Phys. Chem. B*, 1999, **103**, 8940-8943.
43. A. Nattestad, A. J. Mozer, M. K. R. Fischer, Y. B. Cheng, A. Mishra, P. Bäuerle and U. Bach, *Nat. Mater.*, 2010, **9**, 31-35.
44. Z. Liu, D. Xiong, X. Xu, Q. Arooj, H. Wang, L. Yin, W. Li, H. Wu, Z. Zhao, W. Chen, M. Wang, F. Wang, Y. Cheng and H. He, *ACS Appl. Mater. Interfaces*, 2014, **6**, 3448-3454.
45. Z. Liu, W. Li, S. Topa, X. Xu, X. Zeng, Z. Zhao, M. Wang, W. Chen, F. Wang, Y. Cheng and H. He, *ACS Appl. Mater. Interfaces*, 2014, **13**, 10614-10622.
46. H. Hsu, C. Wang, A. Fathi, J. Shiu, C. Chung, P. Shen, T. Guo, P. Chen, Y. Lee and E. W. Diau, *Angew. Chem. Int. Ed.*, 2014, 10-1002.
47. A. Kay and M. Grätzel, *Sol. Energy Mater. Sol. Cells*, 1996, **44**, 99-117.
48. H. Han, U. Bach, Y. Cheng, R. A. Caruso and C. MacRae, *Appl. Phys. Lett.*, 2009, **94**, 103102.
49. H. Wang, G. Liu, X. Li, P. Xiang, Z. Ku, Y. Rong, M. Xu, L. Liu, M. Hu, Y. Yang and H. Han, *Energy Environ. Sci.*, 2011, **4**, 2025-2029.
50. Z. Ku, Y. Rong, M. Xu, T. Liu and H. Han, *Sci. Rep.*, 2013, **3**, 3132.
51. M. Xu, Y. Rong, Z. Ku, A. Mei, T. Liu, L. Zhang, X. Li and H. Han, *J. Mater. Chem. A*, 2014, **2**, 8607-8611.
52. Y. Rong, Z. Ku, A. Mei, T. Liu, M. Xu, S. Ko, X. Li and H. Han, *J. Phys. Chem. Lett.*, 2014, **5**, 2160-2164.
53. A. Mei, X. Li, L. Liu, Z. Ku, T. Liu, Y. Rong, M. Xu, M. Hu, J. Chen, Y. Yang, M. Grätzel and H. Han, *Science*, 2014, **345**, 6194.
54. G. Xing, N. Mathews, S. Sun, S. S. Lim, Y. M. Lam, M. Grätzel, S. Mhaisalkar and T. C. Sum, *Science*, 2013, **342**, 344-347.
55. S. D. Stranks, G. E. Eperon, G. Grancini, C. Menelaou, M. J. P. Alcocer, T. Leijtens, L. M. Herz, A. Petrozza and H. J. Snaith, *Science*, 2013, **342**, 341-344.
56. K. Tanaka, T. Takahashi, T. Ban, T. Kondo, K. Uchida and N. Miura, *Solid State Commun.*, 2003, **127**, 619-623.
57. L. M. Peter, *J. Phys. Chem. C*, 2007, **111**, 6601-6612.
58. H. Kim, I. Mora-Sero, V. Gonzalez-Pedro, F. Fabregat-Santiago, E. J. Juarez-Perez, N. Park and J. Bisquert, *Nat. Commun.*, 2013, **4**, 2242-2248.
59. V. Gonzalez-Pedro, E. J. Juarez-Perez, W. Arsyad, E. M. Barea, F. Fabregat-Santiago, I. Mora-Sero and J. Bisquert, *Nano Lett.*, 2014, **14**, 888-893.
60. A. Dualeh, T. Moehl, N. Tétreault, J. Teuscher, P. Gao, M. K. Nazeeruddin and M. Grätzel, *ACS Nano*, 2014, **8**, 362-373.
61. L. Etgar, P. Gao, Z. Xue, Q. Peng, A. K. Chandiran, B. Liu, M. K. Nazeeruddin and M. Grätzel, *J. Am. Chem. Soc.*, 2012, **134**, 17396-17399.
62. W. A. Laban and L. Etgar, *Energy Environ. Sci.*, 2013, **6**, 3249-3253.
63. J. Bisquert, A. Zaban, M. Greenshtein and I. Mora-Seró, *J. Am. Chem. Soc.*, 2004, **126**, 13550-13559.
64. T. Leijtens, B. Lauber, G. E. Eperon, S. D. Stranks and H. J. Snaith, *J. Phys. Chem. Lett.*, 2014, **5**, 1096-1102.

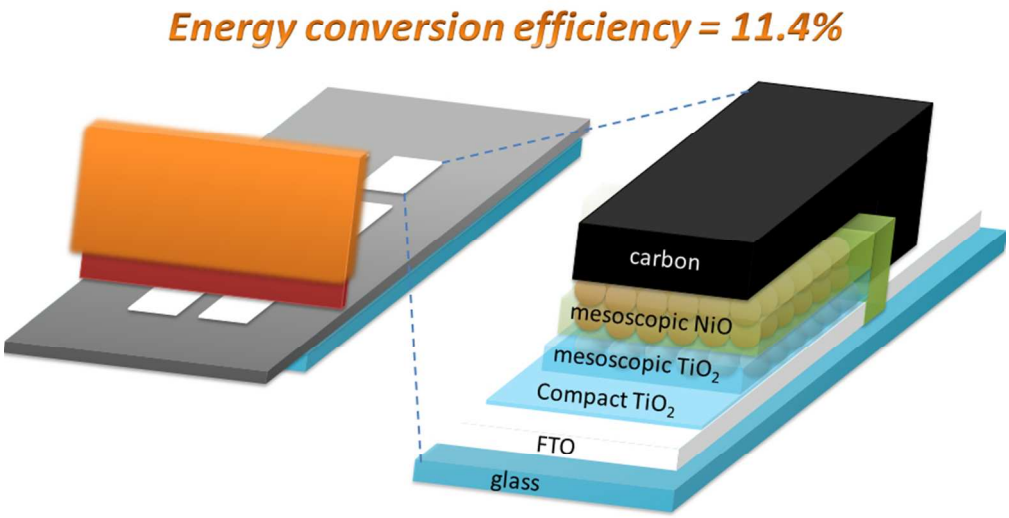

254x190mm (96 x 96 DPI)